American Mineralogist, Volume 93, pages 463–469, 2008

Environmental parameters affect the physical properties of fast-growing magnetosomes

Damien Faivre,[1,*] Nicolas Menguy,[2] Mihály Pósfai,[3] and Dirk Schüler[1,4]

[1]Department of Microbiology, Max Planck Institute for Marine Microbiology, Celsiusstr. 1, 28359 Bremen, Germany
[2]Institut de Minéralogie et Physique des Milieux Condensés, UMR 7590, CNRS, Universités Paris 6 et 7, IPGP, 140 rue de Lourmel, 75015 Paris, France
[3]Department of Earth and Environmental Sciences, University of Pannonia, POB 158, 8200 Veszprém, Hungary
[4]Microbiology, Department of Biology, LMU München, Maria-Ward-Strasse 1a, 80638 München, Germany

Abstract

Magnetotactic bacteria are known to mediate the formation of intracellular magnetic nanoparticles in organelles called magnetosomes. These magnetite crystals are formed through a process called biologically controlled mineralization, in which the microorganisms exert a strict control over the formation and development of the mineral phase. By inducing magnetite nucleation and growth in resting, Fe-starved cells of *Magnetospirillum gryphiswaldense*, we have followed the dynamics of magnetosome development. By studying the properties of the crystals at several steps of maturity, we observed that freshly induced particles lacked a well-defined morphology. More surprisingly, although the mean particle size of mature magnetosomes is similar to that of magnetosomes formed by constantly growing and Fe-supplemented bacteria, we found that other physical properties such as crystal-size distribution, aspect ratio, and morphology significantly differ. Correlating these results with measurements of Fe uptake rates, we suggest that the expression of different faces is favored for different growth conditions. These results imply that the biological control over magnetite biomineralization by magnetotactic bacteria can be disturbed by environmental parameters. Specifically, the morphology of magnetite crystals is not exclusively determined by biological intervention through vectorial regulation at the organic boundaries or by molecular interaction with the magnetosome membrane, but also by the rates of Fe uptake. This insight may contribute to better define biomarkers and to an improved understanding of biomineralizing systems.

Keywords: Biomineralization, magnetotactic bacteria, magnetosomes, magnetite, morphology

Introduction

Bio-induced and bio-controlled mineralization (BIM and BCM, respectively) were historically distinguished on the basis of the process pathway, the crystal properties, and the functionality of the crystals that are formed (Bazylinski and Frankel 2003; Frankel and Bazylinski 2003; Lowenstam 1981). Biomineralization and assembly of bacterial magnetosomes are intracellular processes under strict genetic control (Komeili et al. 2006; Scheffel et al. 2006; Ullrich et al. 2005) that result in magnetite crystals that are strain-specific and have narrow crystal-size distributions (CSDs) (Devouard et al. 1998), enabling the cell to orient itself in magnetic fields (Dunin-Borkowski et al. 1998). Thus, magnetite formation by magnetotactic bacteria (MTB) is generally regarded as a typical example of BCM in prokaryotes.

Information about the dynamics of magnetosome formation at the crystal-chemical as well as at the cellular level has remained sparse while the properties of BCM crystals are well understood. It was shown that magnetosomes can have various morphologies, but that these morphologies are strain-specific (Baeuerlein 2003). Only little variations of the morphologies of elongated crystals were reported for the magnetococcus MC-1, presumably resulting from differences in the growth medium that affected crystal growth rates (Meldrum et al. 1993). However, even in this case, a well-defined morphology was observed for immature crystals, suggesting that the cell exerts control over crystal development even at the early stages of crystal growth.

An extensive knowledge of the dynamics of magnetosome development, correlated with the time-resolved analysis of the evolving magnetosomes, is required for the understanding of the biomineralization process. Thus, to determine how magnetosomes grow and how MTB control the formation of the magnetic inclusions, we used a technique that allowed us to study the dynamics of controlled magnetosome development, without the perturbation caused by cell division (Scheffel et al. 2006). Magnetite formation was induced under controlled conditions in non-magnetic, Fe-starved resting cells by the addition of Fe, and the properties of the crystals [CSDs, shape factor distributions (SFDs), and morphology] were subsequently analyzed at different stages of their growth.

* Present address: Department of Biomaterials, Max Planck Institute of Colloids and Interfaces, Science Park Golm, 14424, Potsdam, Germany. E-mail: damien.faivre@mpikg.mpg.de

MATERIALS AND METHODS

Organism and growth conditions

The magnetotactic bacterium *Magnetospirillum gryphiswaldense* strain MSR-1 (DSM 6361) was used throughout all experiments. This model microorganism can be grown in the laboratory more readily than other MTB (Schleifer et al. 1991). Cells were grown at 28 °C, in a 100 mL medium in 1 L flasks, in microaerobic conditions (1% O_2 in the headspace) (Heyen and Schüler 2003). The medium described in this report was optimized for the growth of cells in an "Fe-free" minimal medium. Compared to the rich medium, components were either omitted or added at lower concentrations (HEPES: 10 m*M*, Na-pyruvate: 27.5 m*M*, $NaNO_3$: 4 m*M*, KH_2PO_4: 0.7 m*M*, $MgSO_4$: 0.6 m*M*, and soy bean peptone: 1 g/L). Iron concentration in the medium was determined by a modified version (Viollier et al. 2000) of the ferrozine assay (Stookey 1970). The total Fe concentration was below the detection limit of 1 μ*M*, which supports cell growth but not the formation of magnetite. This medium was called "low-iron medium" (LIM). "Magnetite-free" cells were obtained after 4 passages in the LIM. For the reference sample, 50 μ*M* Fe^{3+} citrate was added to the LIM.

Non-growing cells

After the establishment of a non-magnetic culture, cells in the mid-logarithmic growth phase were transferred to a low-C medium (LCM)—a medium in which they could not grow but still formed magnetite under the same conditions (28 °C, 100 mL medium in 1 L flasks, microaerobic conditions). The LCM had the same composition as the LIM, except that pyruvic acid sodium salt and peptone were omitted. Under these conditions, cells remained viable as indicated by motility upon microscopic investigation, and retained the potential to biomineralize magnetosomes throughout the experiment as shown by an increase in C_{mag} (Schüler et al. 1995). Briefly, cells were aligned at different angles relative to a light beam by means of an external magnetic field. The ratio of the resulting maximum and minimum scattering intensities (C_{mag}) is correlated with the average number of magnetic particles and can be used for a qualitative assessment of magnetite formation. Magnetite formation was induced by addition of 50 μ*M* Fe^{3+}-citrate to the Fe-starved cells in LCM. Incubation was under the same conditions (28 °C, 1% O_2) as in the LIM growth experiments. Iron uptake rates were determined from the difference of the Fe concentration in the medium between two samplings, normalized by the dry weight of bacteria present in the medium.

Determination of growth and magnetite formation

Bacterial growth was determined by measuring the Optical Density (OD) at 565 nm (Shimadzu UV-1201V spectrophotometer). The magnetic orientation of cells was determined by optical measurements (C_{mag}) (Schüler et al. 1995). Iron was added to the medium at the concentration of 50 μmol/L as Fe^{3+}citrate. At given time intervals, samples of 2.0 mL were withdrawn from the culture for C_{mag} determination, and for the preparation of TEM grids.

Grid preparation and TEM analysis

About 1 mL of the cell suspension was used for grid preparation. The probes were centrifuged at 14000 rpm for 5 min and then resuspended in 100 μL of LIM. Then copper grid with an amorphous carbon support film was deposited on a drop of the preparation and let for about 10 min for adsorption. The grids were subsequently removed, washed with deionized water and dried with filter paper. Bright-field TEM images were obtained with a Zeiss EM10 transmission electron microscope at an accelerating voltage of 60 kV. Inter-particle distances and particle properties were analyzed using standard analytical software for processing digitized electron microscope images (ImageJ) and according to a previously described method (Faivre et al. 2005). Briefly, magnetosome sizes and shape factors were obtained from scanned micrographs. The dimensions were estimated by determining the best fit of an ellipse to the projection of to the particle. The major and minor axes of the best fitting ellipse were used as the length and width of the crystal respectively. This technique has been shown to produce negligible artifacts in the size distributions (Devouard et al. 1998).

HRTEM analysis

Intracellular magnetite crystals were characterized by HRTEM using a JEOL 2100F electron microscope operating at 200 kV. Due to the fact that the crystals are viewed in projection, the shape determination of nanocrystals is not an easy task (Buseck et al. 2001). Since the TEM pole piece allowed us to tilt the sample in the range –20 to +20°, it was neither possible to perform TEM tomography, nor to obtain high-tilt series of images as in (Golden et al. 2004). We have employed a method previously used for a study of pure abiotic magnetites (Faivre et al. 2005). For each particle, the observation zone axis and a crystallographic direction perpendicular to this axis were determined from the 2-D fast Fourier transform (FFT) of the image and the corresponding stereographic projection (Figs. 1a and 1b). This method is based on two points: (1) the knowledge of the crystallographic orientation considerably reduces the number of morphologies compatible with the observed shape; (2) about fifty mature crystals have been studied providing a reasonable statistical basis. Moreover, the habit for MSR-1 magnetosomes is known to be cuboctahedral or close to cuboctahedral. Hence, we compared the observed shape with several models with different expressions of {100}, {111}, and {110} faces (Figs. 1c, 1d, 1e, and 1f). For instance, for the magnetite crystal presented in Figure 1a, it appears that the most probable shape is a cube with poorly developed {110} and {111} faces (Fig. 1g).

RESULTS AND DISCUSSION

We observed the first magnetite-containing cells after 55 min. TEM observations did not reveal any magnetite particle in samples that were taken earlier. Sampling was repeated after 100, 220, and 340 min. Mean particle sizes (±1σ) recorded 100, 220, and 340 min after Fe addition of Fe (hereafter referred to as "immature," "intermediate," and "mature" states) were 19.4 (7.9), 26.3 (9.6), and 31.5 (13.9) nm, respectively. On the other hand, a mean size of 32.5 ± 10.0 nm was measured for crystals that formed in growing cells continuously exposed to Fe-sufficient conditions (hereafter referred to as "reference" state). At least 200 particles were measured in each sample (Table 1). The average numbers of particles per cell (±1σ) were 17.8 (3.7), 20.3 (5.3), and 29.5 (6.1) in immature, intermediate, and mature cells, respectively, whereas it was 32.1 (7.6) in reference cells (40 cells studied). Thus, two conclusions can be drawn from these results: First, and not surprisingly, crystal dimensions continuously increase after addition of Fe; and second, that after 340 min the average size and number per cell of the induced magnetosomes have almost reached the average values that are characteristic of the reference magnetosomes and cells. Thus, the so-called mature magnetosomes definitely have reached a "mature" state of development.

CSDs of the developing crystals at different stages of their growth exhibited distinct changes (Figs. 2a, 2c, and 2e). The CSDs of the magnetosomes from the induced experiments were always positively skewed (skewness of the distributions: 0.26, 0.06, and 0.50 at 100, 220, and 340 min after Fe addition, respectively), but evolved from a nearly normal distribution (at 100 and 220 min) to a broader distribution (340 min) In contrast, reference crystals presented an asymmetric and negatively skewed CSD, with sharp cut-off toward larger sizes (Fig. 2g). Thus, even though the mean particle sizes of mature and reference magnetosomes are similar, their CSDs differ (Figs. 2e and 2g). CSDs of magnetosomes have been tentatively used as biomarkers (Devouard et al. 1998; Faivre et al. 2005; Faivre and Zuddas 2006; Pósfai et al. 2001; Thomas-Keprta et al. 2000), but it has been demonstrated lately that a statistical analysis of sizes and shapes of bio-controlled magnetite particles may not be sufficient to reveal the origin of the crystals (Arató et al. 2005). Nevertheless, the CSD in general gives some hints about the crystal-formation pathway (Eberl et al. 1998). In our experiments, the observed difference between the CSDs of induced mature and referenced particles suggests that the particles originate from two different processes. Specifically, as the CSD of the refer-

TABLE 1. Time-resolved properties of the developing magnetosomes and a comparison with the reference in continuously growing and Fe-supplemented cells (N.A. not applicable, N.D. not determined)

Sample name	Crystallite	Immature	Intermediate	Mature	Reference
Time after induction (min)	55	110	220	340	N.A.
Average size (nm)	N.D.	19.4	26.3	31.5	32.5
Average number of magnetosomes per cell	N.D.	17.8	20.3	29.5	32.1
General morphology	Lack a well-defined morphology	N.D.	N.D.	Dominated by {100} faces	Cubooctahedral

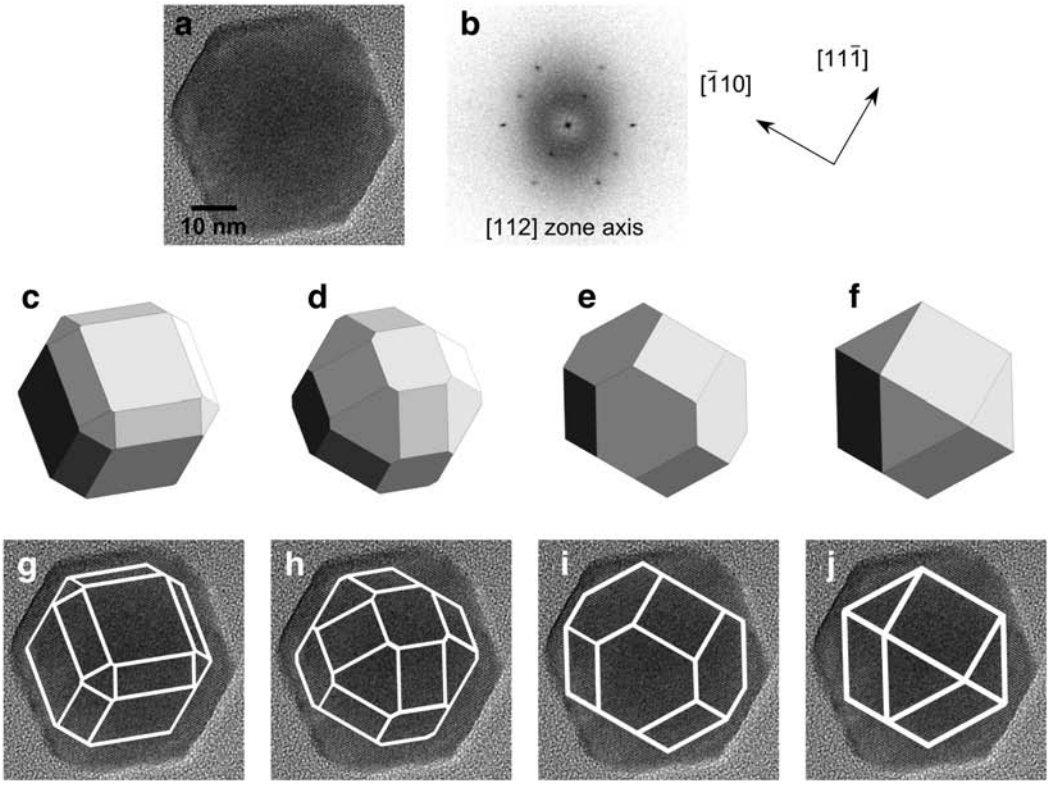

FIGURE 1. (**a**) High-resolution image of an intracellular mature magnetite crystal. (**b**) Fast Fourier transform (FTT) of the image in **a**. As explained in the methodology section, the FFT allows the precise determination of the crystallographic orientation of the particle, as shown next to **b**. (**c**–**f**) Four different morphological models derived from various combinations of the three crystal forms {111} (octahedron), {100} (cube), and {110} (dodecahedron), shown in the same orientation as the magnetite crystal in **a**. (**g**–**j**) The projected outlines of the models are compared with the magnetosome in **a**. The cube with poorly developed {110} and {111} faces in **c** appears to be the most probable morphology, compatible with the studied magnetite crystal (**g**).

ence crystals is narrower than that of mature magnetosomes, the process leading to the formation of the mature magnetosomes is less strictly controlled than the process leading to the development of the reference magnetosomes.

Particles of the freshly induced cells exhibit broad shape factor distributions (SFDs): 30% of the immature magnetosomes are elongated (SF < 0.75), and no distinct maximum can be observed in the SFD. The intermediate and mature crystals have more equidimensional shapes: 54 and 65% of magnetosomes have SF > 0.85 in intermediate and mature cells, respectively, and distinct maxima appear at SF = 0.90 and 0.95, respectively (Figs. 2b, 2d, and 2f). However, the SFD is even narrower for the reference crystals (Fig. 2h), with 93% of the magnetosomes having SF > 0.85 and a maximum at SF = 0.95. The difference between mature and reference magnetosomes presumably confirms the difference observed in the CSDs, i.e., that the crystals did not develop under the same conditions in these two cases. Specifically, as the distribution of the reference crystals is significantly narrower than that of the mature crystals, the reference crystals formed under more-controlled conditions than the magnetosomes that formed in the controlled Fe-induction experiment.

We further attempted to determine the morphologies of the freshly nucleated crystallites (55 min after induction), the mature and the reference magnetosomes (Table 1, Fig. 1 and 3). The habits of the newly formed crystallites can be seen in Figure 3a. Due to the weaker contrast of these small particles with respect to the surrounding cell, the determination of the 3-D shape is particularly difficult. For crystals smaller than 10 nm, a large diversity of shapes was observed, and no unique shape could be clearly distinguished. No structural phase other than magnetite could be detected using electron diffraction, not even a poorly crystalline one. In a previous study on MC-1, it was assumed that the crystals at the end of the magnetosome chain were the youngest and thus the immature particles (Meldrum

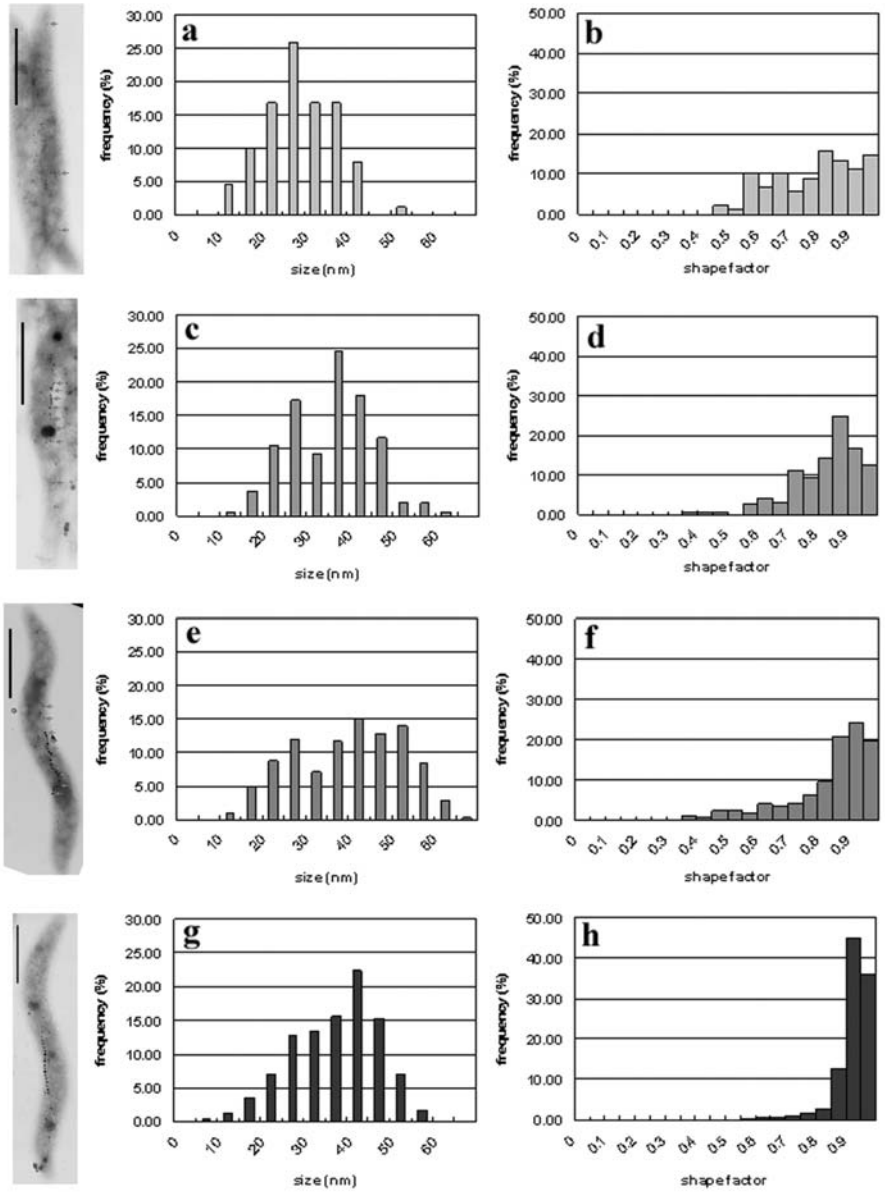

FIGURE 2. CSDs and SFDs (left and right, respectively) of developing magnetosomes. (**a** and **b**) 100 min after induction, (**c** and **d**) 220 min after induction, and (**e** and **f**) 340 min after induction. (**g**) CSD and (**h**) SFD of reference magnetosomes. TEM images of characteristic induced and reference cells are also presented (scale bar = 1 μm).

et al. 1993). In that case, the smallest magnetosomes displayed equidimensional morphologies, unlike the elongated mature crystals. However, as {110} faces were already present on both the small and the mature crystals, those authors concluded that the bacteria acted to control the development of crystal nucleation and growth even at the early stages of crystal growth. In our study, the particles that formed first (55 min after induction) are small and immature, and lack a well-defined morphology (Fig. 3a). This observation confirms our interpretation of CSDs and SFDs that although the nucleation of magnetite in the vesicles is under strict biological control that imposes a chemical supersaturation enabling magnetite formation, the crystal growth process is too fast in our induction experiments for the cells to be able to control the morphology at an early stage.

The morphologies of mature magnetosomes were studied in another set of experiments. For some zone axes, the projected shapes can be modeled by two or three morphologies, preventing the unambiguous determination of the actual 3-D morphologies of the nanoparticles (Fig. 3b). However, some conclusions can be drawn from the observation of about 50 mature magnetite crystals. The morphologies of mature magnetosomes are based on {100}, {110}, and {111} faces, with the majority of the crystals exhibiting relatively large {100} faces, i.e., the crystals resemble cubes with small {110} and {111} faces (Fig. 3b). Cuboocta-hedral particles with similar expression of the {100} and {111} faces were also observed. Thus, although no unequivocal mor-

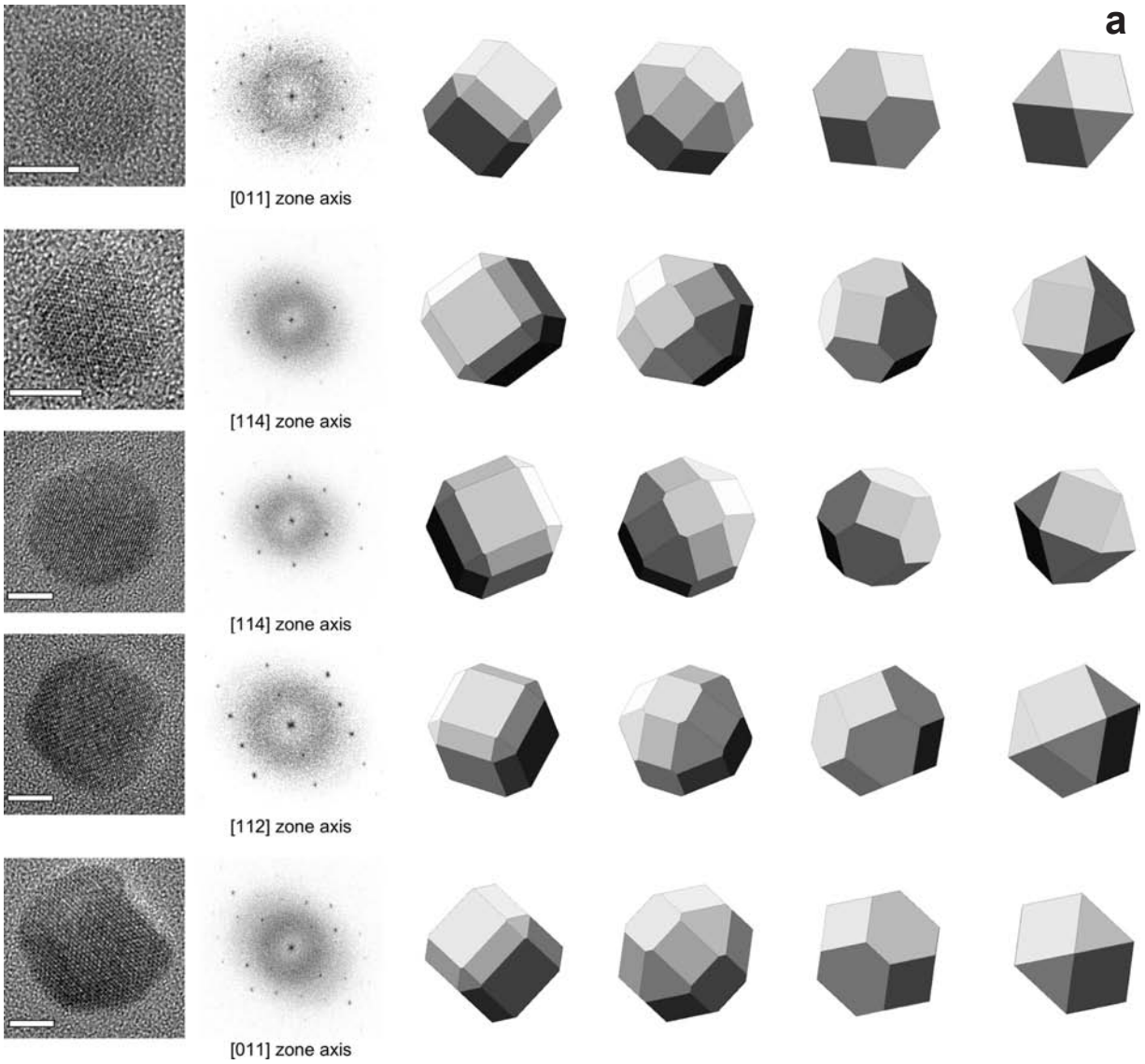

FIGURE 3. Examples of comparisons between the projected shapes of magnetosomes, as observed in HRTEM images, and morphological models that consist of various expressions of the {111}, {100}, and {110} forms. The models are shown in the same orientation as the corresponding magnetosomes, for which the crystallographic orientation was determined from their FFT values (shown in the second column of the figures). (**a**) Crystallites, sampled 55 min after Fe induction (scale bar = 4 nm). The crystallites appear rounded and have irregular shapes, making a meaningful identification of their morphologies impossible. The shapes of the crystallites vaguely match almost any of the idealized model morphologies. (**b**) Mature magnetosomes, sampled 340 min after Fe induction (scale bar = 10 nm). The projected outlines of the magnetosomes are consistent with the cube-like models (**c**) Reference magnetosomes, formed in continuously growing and Fe-supplemented cells (scale bar = 10 nm). The outlines of the magnetosomes and the thickness fringes in their HRTEM images are consistent with the cuboctahedral models.

phology could be determined, most of the mature magnetosomes appear to possess a cube-like shape. The observed variety of morphologies, and their difference from the generally cuboctahedral morphology of magnetosomes from magnetospirilla (Devouard et al. 1998; Mann et al. 1984; Pósfai et al. 2006), indicate that magnetite growth—just as magnetite nucleation—is not under strict biological control in our induction experiments.

From the analysis of about 50 reference magnetosomes, we conclude that the typical habit of the reference MSR-1 crystals is cuboctahedral with {100} faces nearly as large as {111} faces, and little to no expression of {110} faces (Fig. 3c). Thus, the morphologies of the reference magnetosomes are not compatible with most of the observed projections of the mature magnetosomes, as it should be if the classical BCM process was followed. The present study shows that the morphologies of mature magnetosomes can be influenced by experimental conditions. This result suggests that conditions allowing the rapid formation of magnetosomes also have an effect on the morphology of the crystals. Thus, the definition of biomarkers should take into account the possibility for the bacteria to form

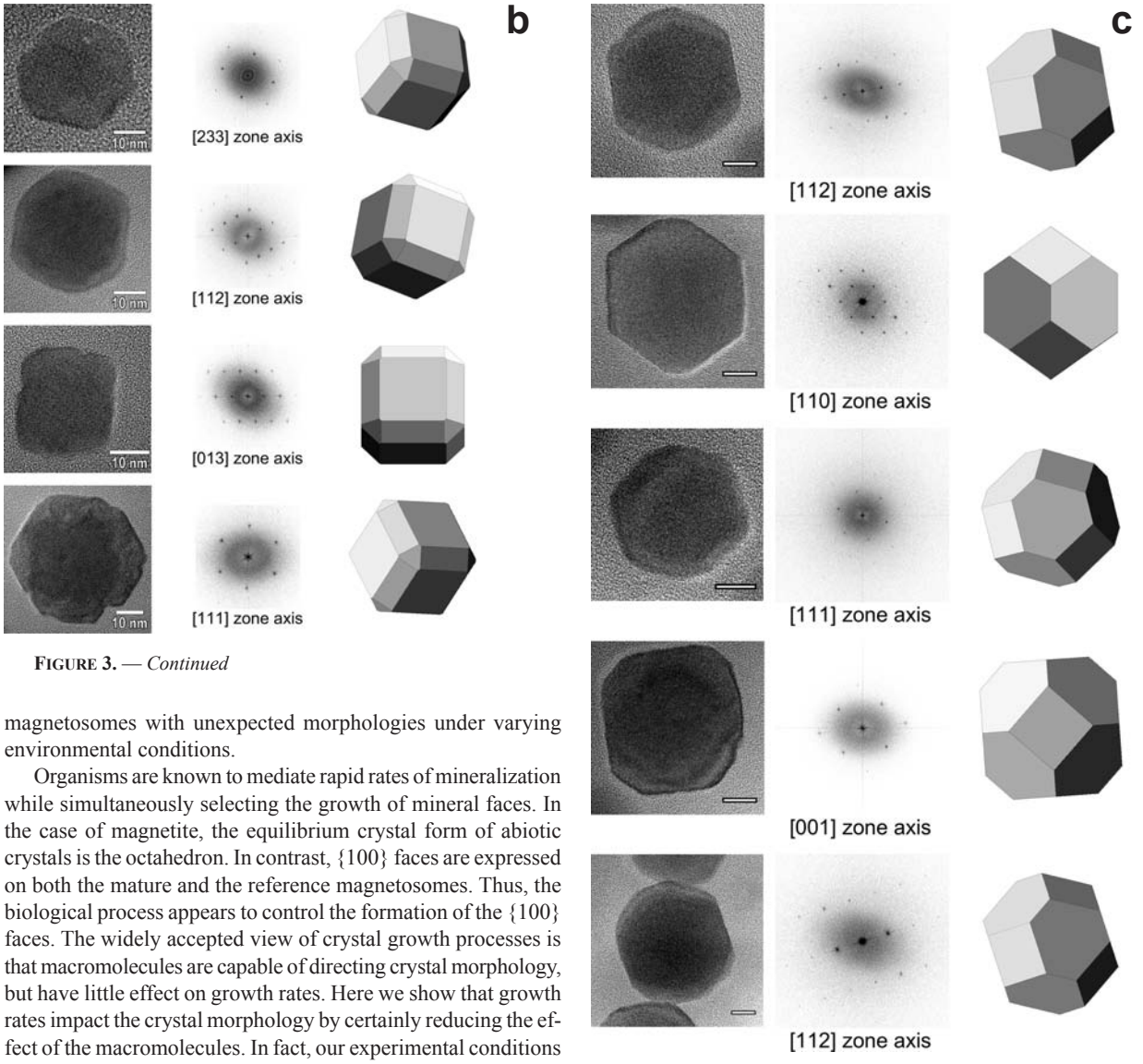

FIGURE 3. — *Continued*

magnetosomes with unexpected morphologies under varying environmental conditions.

Organisms are known to mediate rapid rates of mineralization while simultaneously selecting the growth of mineral faces. In the case of magnetite, the equilibrium crystal form of abiotic crystals is the octahedron. In contrast, {100} faces are expressed on both the mature and the reference magnetosomes. Thus, the biological process appears to control the formation of the {100} faces. The widely accepted view of crystal growth processes is that macromolecules are capable of directing crystal morphology, but have little effect on growth rates. Here we show that growth rates impact the crystal morphology by certainly reducing the effect of the macromolecules. In fact, our experimental conditions enabled the formation of mature magnetosomes in less than 6 h, whereas the formation of the reference magnetite crystals was observed after 24 h. We measured up to 30 $nmol_{Fe}$/min per mg dry weight Fe uptake during magnetosome formation by induced cells, whereas growing and permanently Fe-supplemented cells on average used 1 $nmol_{Fe}$/min per mg dry weight, which shows more than one order-of-magnitude difference in Fe uptake rate at a given time (Fig. 4). Because {100} faces were dominant in the induction experiments, the growth rate along <100> had to be smaller than along <111>. In contrast, in the reference sample, {111} faces were observed to be largest, indicating that the growth rate along <100> exceeded that along <111>. It has to be noted that the differences in the media may impact the physiology of the cells that in turn can have an effect on the observed morphology. In any case, the expression of different faces is favored for different growth conditions. Similar observations were made on calcite crystals where it was shown that different crystallographic forms had different isotopic signatures, reflecting different growth rates (Dickson 1991). Thus, it will be extremely interesting to study the isotopic properties of the magnetite crystals formed under these different conditions in future experiments.

In summary, we propose that the process of magnetosome formation proceeds as follows. During the initial phase, magnetite crystals nucleate under chemical supersaturation conditions controlled by the bacteria. Local supersaturation could be achieved, for example, by the effect of an Fe-transport protein such as MamM or MamB (Jogler and Schüler 2006), or an acidic protein such as Mms6 (Arakaki et al. 2003), which concentrate the iron. Another possibility is based on the fact that magnetite crystallites were shown to be membrane-associated, and thus the protein may also serve as a nucleation site (Faivre et al. 2007).

The nucleation process results in normal CSDs and irregular morphologies. These physical properties suggest that magnetosome formation cannot be strictly biochemically controlled, at least when the rate of Fe uptake is large. During a later phase, the rate of Fe transport to the magnetosomes decreases, resulting

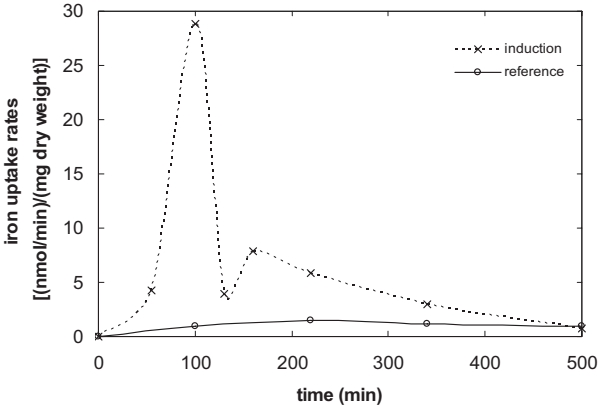

FIGURE 4. Iron uptake rates during the induction experiments (crosses and dashed line) and comparison with reference experiments (open circles and continuous line). After 100 min, the rates are ~30× larger in the induction experiments than in the reference experiment. Then the rates are slowing down and the values are similar in the two experiments after 500 min.

in a more-controlled growth of the magnetosomes that reach the magnetic single-domain size. Alternatively, the Fe flux might remain constant, but the increase in particle surface area could be sufficient to reduce particle growth rates. Depending on the external Fe concentration, magnetosome formation can be rapid, generating a morphology resembling a cube; or slower, producing then the classical cubooctahedral morphology.

These findings show that bio-controlled mineralization processes that are currently used to reconstruct paleoenvironments are not necessarily robust parameters as they can be influenced by external factors. This suggests a key role for Fe uptake rates in BCM together with genetic control by the organism, as the BCM pathway and the resulting crystal properties are not necessarily unique and can exhibit some variations. Finally, these findings provide an avenue for understanding biomineralization at the physico-chemical level and designing biomimetic approaches that will enable formation of magnetite with a degree of control only expressed in biominerals.

ACKNOWLEDGMENTS

This research was supported by the Max Planck Society and the Biofuture program of the BMBF. D.F. acknowledges support from a Marie Curie Fellowship from the European Union (BacMag, EIF-2005-009637), and M.P. received support from the Hungarian Research Fund (OTKA-48607).

REFERENCES CITED

Arakaki, A., Webbs, J., and Matsunaga, T. (2003) A novel protein tightly bound to bacterial magnetite particles in *Magnetospirillum magnetotacticum* Strain AMB-1. Journal of Biological Chemistry, 278(10), 8745–8750.

Arató, B., Szanyi, Z., Flies, C.B., Schüler, D., Frankel, R.B., Buseck, P.R., and Pósfai, M. (2005) Crystal-size and shape distributions of magnetite from uncultured magnetotactic bacteria as a potential biomarker. American Mineralogist, 90, 1233–1241.

Baeuerlein, E. (2003) Biomineralization of unicellular organisms: An unusual membrane biochemistry for the production of inorganic nano- and microstructures. Angewandte Chemie International Edition, 42(6), 614–641.

Bazylinski, D.A. and Frankel, R.B. (2003) Biologically controlled mineralization in prokaryotes. In P.M. Dove, J.J. De Yoreo, and S. Weiner, Eds., Biomineralization, 54, p. 217–247. Reviews in Mineralogy and Geochemistry, Mineralogical Society of America, Chantilly, Virginia.

Buseck, P.R., Dunin-Borkowski, R.E., Devouard, B., Frankel, R.B., McCartney, M.R., Midgley, P.A., Posfai, M., and Weyland, M. (2001) Magnetite morphology and life on Mars. Proceedings of the National Academy of Sciences of the U.S.A., 98(24), 13490–13495.

Devouard, B., Pósfai, M., Hua, X., Bazylinski, D.A., Frankel, R.B., and Buseck, P.B. (1998) Magnetite from magnetotactic bacteria: Size distributions and twinning. American Mineralogist, 83, 1387–1398.

Dickson, J.A.D. (1991) Disequilibrium carbon and oxygen isotope variations in natural calcite. Nature, 353, 842–844.

Dunin-Borkowski, R.E., McCartney, M.R., Frankel, R.B., Bazylinski, D.A., Pósfai, M., and Buseck, P.R. (1998) Magnetic microstructure of magnetotactic bacteria by electron holography. Science, 282, 1868–1870.

Eberl, D.D., Drits, V.A., and Srodon, J. (1998) Deducing growth mechanisms for minerals from the shapes of crystal size distributions. American Journal of Science, 298, 499–533.

Faivre, D. and Zuddas, P. (2006) An integrated approach for determining the origin of magnetite nanoparticles. Earth and Planetary Science Letters, 243, 53–60.

Faivre, D., Menguy, N., Guyot, F., Lopez, O., and Zuddas, P. (2005) Morphology of nanomagnetite crystals: Implications for formation conditions. American Mineralogist, 90, 1793–1800.

Faivre, D., Boettger, L., Matzanke, B., and Schüler, D. (2007) Intracellular magnetite biomineralization in bacteria proceeds via a distinct pathway involving membrane-bound ferritin and ferrous iron species. Angewandte Chemie International Edition, 46, 8495–8499.

Frankel, R.B. and Bazylinski, D.A. (2003) Biologically induced mineralization by bacteria. In P.M. Dove, J.J. De Yoreo, and S. Weiner, Eds., Biomineralization, 54, p. 95–114. Reviews in Mineralogy and Geochemistry, Mineralogical Society of America, Chantilly, Virginia.

Golden, D.C., Ming, D.W., Morris, R.V., Brearley, A.J., Lauer Jr., H.V., Treiman, A.H., Zolensky, M.E., Schwandt, C.S., Lofgren, G.E., and McKay, G.A. (2004) Evidence for exclusively inorganic formation of magnetite in Martian meteorite ALH84001. American Mineralogist, 89, 681–695.

Heyen, U. and Schüler, D. (2003) Growth and magnetosome formation by microaerophilic *Magnetospirillum* strains in an oxygen-controlled fermentor. Applied Microbiology and Biotechnology, 61, 536–544.

Jogler, C. and Schüler, D. (2006) Genetic analysis of magnetosome biomineralization. In D. Schüler, Ed., Magnetoreception and magnetosomes in bacteria, p. 133–161. Springer, Heidelberg.

Komeili, A., Li, Z., Newman, D.K., and Jensen, G.J. (2006) Magnetosomes are cell membrane invaginations organized by the actin-like protein MamK. Science, 311(5758), 242–245.

Lowenstam, H.A. (1981) Minerals formed by organisms. Science, 211(4487), 1126–1131.

Mann, S., Frankel, R.B., and Blakemore, R.P. (1984) Structure, morphology and crystal growth of bacterial magnetite. Nature, 310, 405–407.

Meldrum, F.C., Mann, S., Heywood, B.R., Frankel, R.B., and Bazylinski, D.A. (1993) Electron-microscopy study of magnetosomes in a cultured coccoid magnetotactic bacterium. Proceedings of the Royal Society of London. Series B, Biological Sciences, 251(1332), 231–236.

Pósfai, M., Cziner, K., Marton, E., Buseck, P.R., Frankel, R.B., and Bazylinski, D.A. (2001) Crystal-size distributions and possible biogenic origin of Fe sulfides. European Journal of Mineralogy, 13, 691–703.

Pósfai, M., Kasama, T., and Dunin-Borkowski, R.E. (2006) Characterization of bacterial magnetic nano-structures using high-resolution transmission electron microscopy and off-axis electron holography. In D. Schüler, Ed., Magnetoreception and Magnetosomes in Bacteria, p. 197–225. Microbiology Monographs 3, Springer, Heidelberg.

Scheffel, A., Gruska, M., Faivre, D., Linaroudis, A., Plitzko, J.M., and Schüler, D. (2006) An acidic protein aligns magnetosomes along a filamentous structure in magnetotactic bacteria. Nature, 440(7080), 110–115.

Schleifer, K.-H., Schüler, D., Spring, S., Weizenegger, M., Amann, R., Ludwig, W., and Köhler, M. (1991) The genus *Magnetospirillum gen. nov.*, description of Magnetospirillum gryphiswaldense sp. nov. and transfer of Aquaspirillum magnetotacticum to *Magnetospirillum magnetotacticum comb. nov.* Systematic and Applied Microbiology, 14, 379–385.

Schüler, D., Uhl, R., and Baeuerlein, E. (1995) A simple light scattering method to assay magnetism in *Magnetospirillum gryphiswaldense*. FEMS Microbiology Letters, 132, 139–145.

Stookey, L.L. (1970) Ferrozine—A new spectrophotometric reagent for iron. Analytical Chemistry, 42(7), 779–781.

Thomas-Keprta, K.L., Bazlinski, D.A., Kirschvink, J.L., Clemett, S.J., McKay, D.S., Wentworth, S.J., Vali, H., Gibson Jr., E.K., and Romanek, C.S. (2000) Elongated prismatic crystals in ALH84001 carbonate globules: Potential Martian magnetofossils. Geochimica et Cosmochimica Acta, 64(23), 4049–4081.

Ullrich, S., Kube, M., Schübbe, S., Reinhardt, R., and Schüler, D. (2005) A hypervariable 130-kilobase genomic region of magnetospirillum gryphiswaldense comprises a magnetosome island which undergoes frequent rearrangements during stationary growth. Journal of Bacteriology, 187(21), 7176–7184.

Viollier, E., Inglett, P.W., Hunter, K., Roychoudhury, A.N., and Van Cappellen, P. (2000) The ferrozine method revisited: Fe(II)/Fe(III) determination in natural waters. Applied Geochemistry, 15(6), 785–790.

MANUSCRIPT RECEIVED APRIL 23, 2007
MANUSCRIPT ACCEPTED SEPTEMBER 21, 2007
MANUSCRIPT HANDLED BY HONGWU XU